HEFAT2011
8th International Conference on Heat Transfer, Fluid Mechanics and Thermodynamics
11 – 13 July 2011
Pointe Aux Piments, Mauritius

EXPERIMENTAL ANALYSIS AND NUMERIC SIMULATION OF STEADY STATE FLOW FORCES ON VALVES OF MECHATRONIC PRESSURE REGULATORS FOR NATRUAL GAS POWERED COMBUSTION ENGINES

Hübner D. H., Klein C. and Ortwig H.*
*Author for correspondence
Department of Mechanical Engineering
Trier University of Applied Siences
P. O. Box 1826, 54208 Trier
Germany
E-mail: huebner.dirk@gmx.de, ortwig@fh-trier.de

ABSTRACT

This paper deals with the experimental analysis and numerical simulation regarding the flow forces of a mechatronical pressure regulator for natural gas powered internal combustion engines.

For the experimental analysis a measurement device was constructed to determine these forces as well as other global flow parameters by variation of the pressure ratio and the strokes of the valve gate.

The series of tests were simulated on the basis of the Computational Fluid Dynamics (CFD)-code FLUENT. Thereby the model was validated through the comparison of the results deriving from the experimental analysis and the results provided by the numerical simulation. It was shown that the flow forces have a strong dependence on the pressure ratio but are not influenced by the mass flow rate. Accordingly the flow forces are independent of the stroke.

By the use of the numerical simulation a visualization of the inner flow characteristics was obtained. Thus the potential for an improvement in the geometry was derived. Besides a generation of eddies in the low and high pressure chamber, backflow occurred in the valve bung as a result of shocks. This took place at low pressure ratios and resulted in a decreasing flow coefficient due to contraction and deceleration of the fluid entering the control edge. At high pressure ratios, a relocation of the flow contraction towards the theoretical flow cross sectional area and a decreasing of the generation and impact of eddies in the valve bung were detected.

INTRODUCTION

Long-term support programmes at the federal and Land level, financial incentives from regional power supply companies and increasing environmental awareness on the part of the consumer point to a growing appeal of natural gas powered motor vehicles in Germany. Indeed, for the purposes of compliance with EU air quality targets and reduced exhaust emissions, natural gas vehicles (NGVs) can make an important contribution as they release much less pollution and noise in the combustion process compared to conventional fuels such as petrol and diesel. The exponential growth in the number of natural gas vehicles now on the road confirms this alternative fuel trend.

Concurrently with this development, technical requirements on the components of the gas management system are becoming more exacting. The central module of this system is the pressure regulator which reduces the output pressure of the gas storage vessel(s) to a level acceptable for injection into the respective intake pipe. The mechanical regulators employed to date are of limited usefulness in cars because of their dynamic response deficiencies and insufficient accuracy. System-inherent drawbacks resulting from the diminishing supply pressure and variable volumetric demand have prompted the development of a mechatronic pressure regulator. Its mechanical operating principle is supplemented by a sensor system detecting the input pressure plus an actuator assembly controlling the plunger. The system thus formed is managed by a processor integrated into the engine control unit.

A key factor influencing the control characteristics of a pressure regulator consists in the reaction forces acting on the plunger as a result of fluid flow past the control edge. The experimental investigation and numerical simulation of these so-called flow forces form the subject of the present research.

NOMENCLATURE

$A_{s(x)}$	[m²]	Flow Cross-Section
$d_{m(x)}$	[m]	Middle Diameter
$l_{(x)}$	[m]	Lateral Cord
D	[m]	Valve Bore Diameter
$d_{(x)}$	[m]	Diameter of Lateral Area
x	[m]	Valveposition
β	[°]	Cone Angle

I_A	[kg m/s]	Outgoing Impetus
I_E	[kg m/s]	Incoming Impetus
$F_{flow,ax}$	[N]	Axial Flow Force
π_{krit}	[-]	Critical Pressure Ratio
κ	[-]	Isentropic Enexponent (air)
p_{vc}	[bar]	Critical Pressure at Vena Contracta
p_1	[bar]	Pressure High-Pressure Chamber
p_2	[bar]	Pressure Low-Pressure Chamber
Ma	[-]	Mach Number

CONCEPTUAL FORMULATION

Designing a mechatronic pressure regulator for the fuel systems of natural gas powered internal combustion engines requires an understanding of the forces acting on the regulator's plunger so that the associated actuating system can be effectively configured. Unfortunately, no useful quantitative data serving our present purpose can be found in the literature. For this reason – and in order to study the flow-induced forces on the plunger, the regulator's internal flow characteristics, and meaningful approaches towards flow geometry improvement – it was decided to conduct a numerical simulation of the steady-state flow forces using the FLUENT software.

The overall objective was to characterize the parameters influencing the flow forces to which the plunger of a mechatronic pressure regulating valve is subjected. To this end, our research was broken down into a design part, an experimental part and a simulation part which can be described as follows:

- The design part comprises the design of the measuring rig, taking into account the flow geometry presented below. The aim was to map the flow field in quantitative terms at defined points of the domain by means of an existing sensor system.
- In the experimental part, the flow force – as well as selected other parameters – within the flow domain were to be determined at variable supply pressures and constant counterpressure for different strokes of the control element.
- In the simulation part, the results of the experimental part were to be validated by numerical flow simulation (taking into account the compressibility of the gas) so as to confirm the validity of the model. Using these results and the internal flow characteristics obtained by simulation, first solution approaches were then to be derived with a view to optimizing the flow geometry. Following the successful verification phase, simulated geometry modifications yielded suggestions for geometrical optimization. Designers are thus provided, for use in their future work, with information on the magnitude of flow forces occurring in the systems examined.

THEORETICAL FLOW FORCES

The flow forces are of key importance even in a preliminary development of pressure regulator valves with a view to improving control performance and reducing valve actuating cycles. The maximum flow force and its evolution as a function of the valve stroke, pressure differential and volumetric flow rate are essential criteria in valve design. On the one hand, the plunger positioning force must be rated with this parameter in mind; on the other hand, the dynamic stability of the control system is influenced by it. This state of affairs complicates the control operation and may result, in the worst case, in oscillation of the system [1].

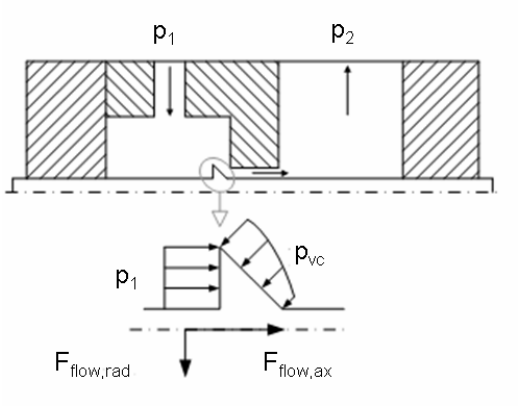

Figure 1: Valve Geometry and Flow Forces

Upon entering the regulator, the fluid passes the control edge which obstructs and thereby restricts the flow. According to Bernoulli's energy equation, an acceleration of the fluid accompanied by a drop in static pressure will occur in this zone. As a result, the pressure acting on the surface area of the plunger cone will be lower than that acting on the adjoining perpendicular surface. The latter is subject to a constant pressure distribution as it remains uninfluenced by the effect described above. The pressure differential generates a force which acts in the closing direction and is referred to as the steady-state portion of the flow force. Being proportional to the stroke of the control element, it acts like a spring force and influences the valve's dynamic properties; it may thus give rise to unstable system behaviour. Any formation of such radial forces should be avoided since they might cause the plunger to bind due to friction in the guide. Generally, however, they will not occur in the first place, given the symmetry of the assembly. However, in the event of a change in volume flow over time, e.g., due to valve switching action, an additional (second) flow force component will be generated, i.e., the non-steady portion. It actually consists of an inertia force which accelerates the air column in the valve chamber. This dynamic component is proportional to the control element's stroke speed and influences the valve's damping behaviour as a function of the inflow direction [2].

The geometry of the cross-section of flow has a major influence on the magnitude of the flow forces. As a general rule, we can distinguish this geometry into a geometrical and a real cross-section of flow. The flow geometry of the valve examined in this research is illustrated in Fig. 2.

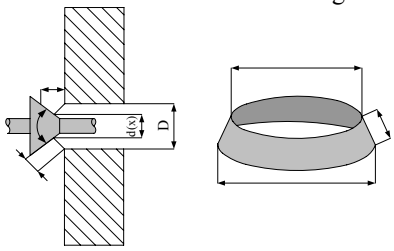

Figure 2: Seat Geometry and Cross Section of Flow Area

The flow cross-section A_s corresponds to the lateral area of a truncated cone and is largely a function of the stroke x:

$$A_S(x) = \pi \cdot d_m(x) \cdot l(x) \tag{1}$$

The mean diameter d_m and the chord length l can be calculated using the following equations:

$$d_m(x) = \frac{D + d(x)}{2} \tag{2}$$

$$l(x) = x \cdot \sin(\beta/2) \tag{3}$$

Using some trigonometry, the stroke-related diameter $d_{(x)}$ can be written as follows:

$$d(x) = D - (\cos(\beta/2) \cdot \sin(\beta/2) \cdot x) \tag{4}$$

Substituting Eq. 2 - 4 into Eq. 1 yields the following equation for the cross-section of flow:

$$A_S(x) = \pi \cdot [D - (\cos(\beta/2) \cdot \sin(\beta/2) \cdot x)] \cdot x \cdot \sin(\beta/2) \tag{5}$$

In the following mathematical explanations an axial reaction force F_{ax} is introduced. This force is counterdirectional to the flow force F_{str} and inhibits axial shifting of the control element during passage of the flow. Thus, the following is required to apply:

$$F_{ax} = F_{flow,ax} \tag{6}$$

In the following discussions it is assumed that we are dealing with a constant pressure system, i.e., the pressures upstream and downstream of the valve are taken to remain constant irrespective of the plunger position. Moreover, the flow forces are determined with reference to a defined control space which, on principle, is freely selectable. In the present case its boundary passes through the narrowest point of the flow cross-section (the so-called "vena contracta") and through the outlet. The equations for calculating the steady-state flow forces are derived on the basis of the momentum equation. Accordingly, the following must hold true:

The sum total of all momentum fluxes passing over the control surface must be equal to the sum of all external forces acting on the control surfaces [3].

$$\sum \vec{F} = \sum \dot{\vec{I}} = \dot{\vec{I}}_A - \dot{\vec{I}}_E \tag{7}$$

Fig. 3 describes the steady-state flow forces at one leading edge. Assuming that $\varphi_2 = 90°$, the following is then obtained for the axial flow force $F_{flow,ax}$:

$$F_{flow,ax} = \rho_E \cdot Q_E \cdot c_E \cdot \cos\varphi_1 \tag{8}$$

From the equation derived above, it is evident that the steady component of the flow force acts on the plunger in a positive x-direction only.

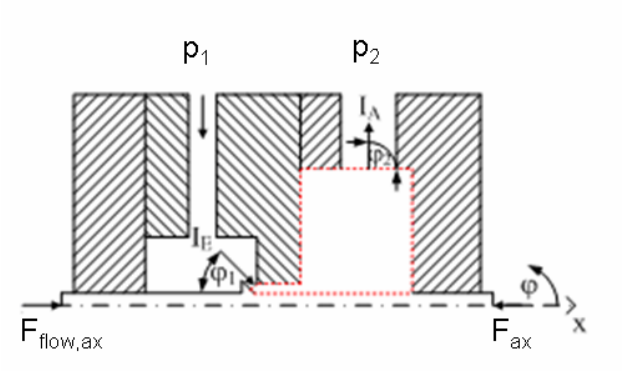

Figure 3: Flow and Impuls

EXPERIMENTAL ANALYSES

For verification of the numerical simulation results, a measuring rig was built. It was to be used chiefly to measure the flow forces at variable supply pressures and constant counterpressure for different strokes of the control element. Moreover, wall pressure and temperature measurements were taken at selected points of the flow domain in order to validate the simulation results. To facilitate further measurements with a view to subsequent geometry variations, a modular design of the measuring rig was adopted.

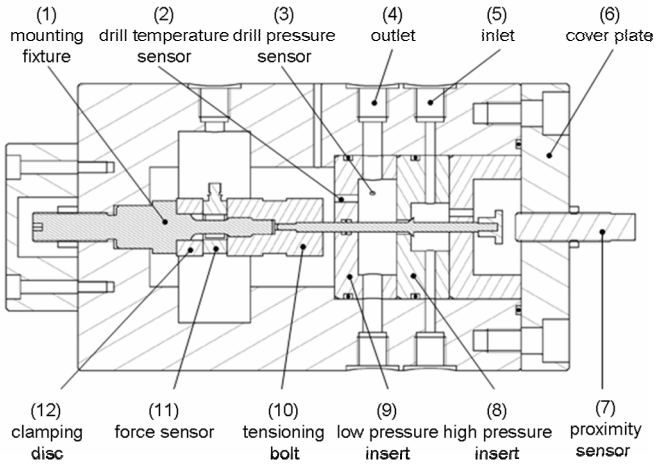

Figure 4: Measuring Device

The discs (8,9) in the base body define the flow space geometry for the high and low pressure chamber. The dimensions of that flow space were obtained in prior research [4]. Given the different internal tube diameters on the high and low pressure sides, the inlet and outlet diameters were selected accordingly.

Inside the high and low pressure chambers, static wall pressure measurements were taken at two points in each case. To this end, a bored passage (3) through the disc and the base body connects the flow space to the pressure transducers

mounted on the periphery of the sleeve. Moreover, a thermocouple (2) is adhesive-bonded into each of the discs (8,9) for measuring the temperature in the respective chamber.

The axial flow force was measured by means of a piezoelectric force sensor (11) which, according to the manufacturer's instructions, needs to be fitted with a special mounting fixture (1) in the form of an expansion screw. The tensioning bolt (10) and the clamping disc (12) between which the force sensor is tensioned must be of an adequate thickness to provide enough stiffness for biasing the sensor. Load measurements can thus be carried out in both the tension and pressure direction, i.e., a flow reversal capability is obtained. Any transverse forces arising are absorbed by adequate prestressing but not measured.

A precise adjustment of the plunger stroke is achieved via the fine thread on the mounting fixture; the setting is locked by tightening a hex nut. The proximity sensor (7) fitted on the lid ensures an adequate positioning of the plunger; however, this sensor had to be removed for the measurements due to its pressure sensitivity. Given the inadequate linearity of the proximity sensor, an angular scale was fitted on the baseplate for cross-checking purposes.

For the quantitative determination of the flow field, sensors were fitted at defined points. Control of the test rig as well as the acquisition and analysis of measured data were ensured by the DIADEM V10.0 software and appropriate National Instruments hardware. The experimental investigation was carried out in the Pneumatics Laboratory of the Trier University of Applied Sciences. Fig. 5 shows the test set-up during a measurement. The proximity sensor is not in place because of its pressure sensitivity.

The experiments were conducted as follows. By opening the gas cylinders (12), the system can be pressurized. While the supply pressure is set with the aid of the pressure regulator (10), the counterpressure is adjusted using the variable flow restrictor (1). Once a steady state is achieved, the data measurement and recording processes are initiated. The measurement series were structured such that the flow force and the global parameters 'pressure', 'temperature' and 'mass flow' were determined for pressure ratios of 16/11, 21/11, 26/11, 31/11, 36/11 and 41/11 bar at a plunger stroke of 0.05 mm, 0.1 mm, 0.15 mm and 0.2 mm in each case.

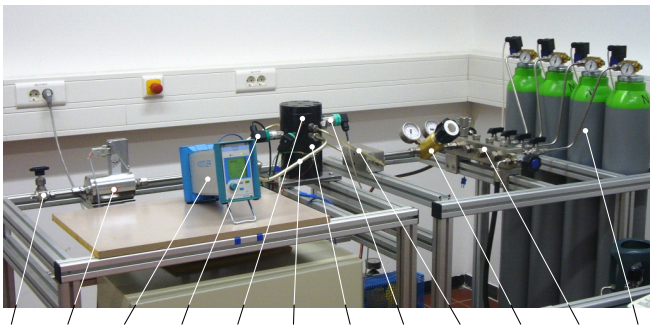

Figure 5: Test Rig – Fluid Power Department
Trier University of Applied Sciences

For reasons of technical safety the measurements were carried out with compressed air. A correction factor was introduced to permit a conversion of the measurement readings, thus ensuring their applicability to the fluid employed in NGV vehicles (i.e., natural gas).

Item	Description
(1)	Variable Flow Restrictor
(2)	Mass Flow Sensor
(3)	Charge Meter
(4)	Pressure Transducer – Low Pressure
(5)	Temperature Sensor – High Pressure
(6)	Low Pressure Line
(7)	Temperature Sensor – Low Pressure
(8)	Pressure Transducer – High Pressure
(9)	High Pressure Line
(10)	Pressure Regulator
(11)	Manifold
(12)	High Pressure Storage Vessel

With a view to ensuring the repeatability of the measured data, five measurements were carried out for each pressure ratio at a defined plunger stroke. The data obtained from each measurement series was subjected to statistical analysis and subsequently visualized using the MATLAB software.

VERIFICATION OF THE CFD-MODEL

In order to demonstrate the validity of the simulation model, the experimental results were compared with those produced by the numerical simulation for the volume flow rates, flow forces and flow coefficients determined. In the following diagrams, measurement readings are in each case represented by squares while the corresponding simulation results are shown as round points.

Volume Flow Rate

Fig. 6 shows a graphic comparison of the measured and simulation results for the volume flow rate at standard conditions as a function of the supply pressure (parameter: plunger stroke in mm).

Except for the 0.15 mm plunger stroke, the simulation results coincide very well with the measured data. The deviation in the 0.15 mm measurement series might be due to a faulty spindle adjustment and should be examined in a follow-up project.

Since a very good match is obtained nevertheless, the model is deemed to be accurate at this point in terms of the calculated volume and mass flow rates at standard conditions, and it is thereby considered validated.

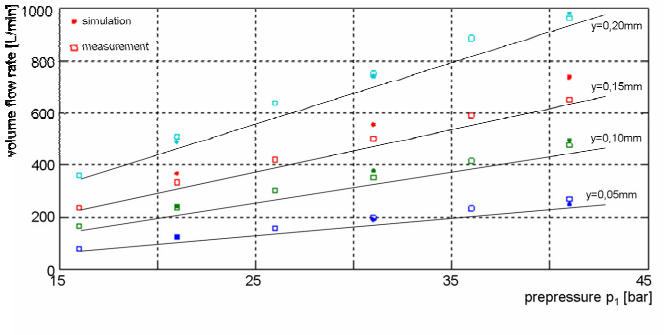

Figure 6: Comparison Volume Flow Rates

Flow Forces

Fig. 7 presents the axial flow forces as a function of the plunger stroke (parameter: supply pressure in bar). Since the experimental results for the 0.05mm stroke setting were not repeatable, they were not included in the appropriate measurement series.

The absolute value deviations observed with increasing pressure ratios can be attributed to system friction (mainly friction forces associated with the O-ring feed-through, which cannot be trivially determined) as well as to potential inaccuracies in the calibration of the charge meter. This leaves some scope for improvement in the context of a subsequent revision of the test rig design.

The force simulation tends to coincide with the measurement readings, so again the model can be deemed valid in this regard.

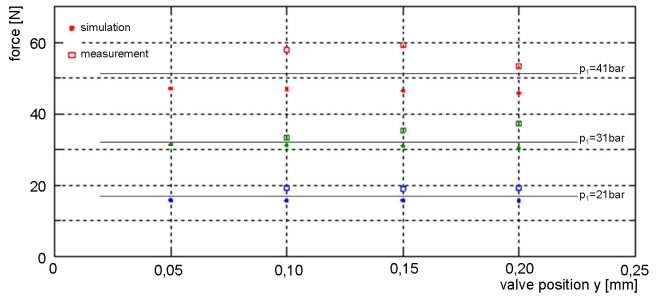

Figure 7: Comparison Valve Forces

Flow Coefficient

Fig. 8 plots the flow coefficients as a function of the supply pressure (parameter: plunger stroke in mm). This characteristic variable represents the ratio of the experimentally determined and simulated mass flow, respectively, to the theoretical maximum mass flow. It thus constitutes a evaluation criterion for the quality of a given flow geometry.

Except for the 0.15 mm measurement series where a faulty spindle adjustment is assumed to have impaired the measurements, a comparison of the simulation and measurement results reveals a good coincidence so that the model can be deemed validated in this respect as well.

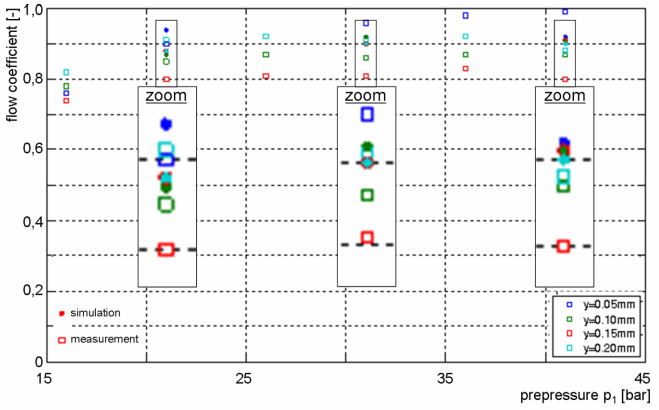

Figure 8: Comparison Flow Coefficients

Result

As was to be expected, the volume flow rate obtained for a constant plunger position exhibits a linear dependence on the gas supply pressure. Minor fluctuations may be a result of geometrical or position variations within the measuring rig, or of temperature variations occurring in the course of the measurement. On principle, the results reflect the actual correlations. The flow forces exhibit a substantial dependence on the pressure differential across the restriction zone but are nearly independent on the plunger stroke and hence, on the mass flow transmitted. Consequently, the analytical description of flow forces known from oil hydraulics need not be adduced in applications of high-pressure valve technology involving gases. A momentum balance will yield much lower values, given the substantially lower density of the fluid (compared to oil or water, the latter is lower by a factor of almost 1000). A modelling approach should be based on a description of the pressure distribution over the valve cone and the adjoining perpendicular annulus surface, the so-called deflector plate. Summing up, it may be stated that for the present geometry and considered as a function of mass flow, the flow forces may in good approximation be considered constant.

The high flow coefficients are indicative of an advantageously selected flow geometry. With increasing supply pressure the flow coefficient rises; however, it asymptotically approaches a constant value. Its dependence on the restriction zone geometry and the prevailing pressure ratio, as noted in [5], is confirmed.

FLOW CHARACTERISTICS

In order to gain a basic understanding of the internal flow processes and associated influencing parameters, a description of the system's internal flow characteristics is given in the following section.

Given the high compressibility of the medium, its consistently turbulent and supercritical passage through the valve is marked by frequent changes in velocity from subsonic to supersonic, as well as by the resulting localized expansion and compression zones characterized by high density, temperature and pressure gradients.

A knowledge of the complex interior flow conditions and of the above-described fluid dynamic phenomena forms the basis

for any optimization of the flow geometry aimed at a reduction of flow forces, pressure losses and loss-inducing dead spaces. Simulation-assisted geometry modifications and parameter variations can then be employed to achieve an efficient quality and performance improvement.

Shock

For the investigations conducted in this research project, the Mach number Ma emerges as being particularly suitable for an interpretation of the simulation result. On the one hand, this dimensionless quantity delimits the subsonic (Ma<1) from the supersonic (Ma>1) range; on the other, regions of high temperature, density or pressure variations can be locally analyzed on the basis of its distribution.

By way of example, Fig. 9 illustrates the Mach number distribution and the static pressure over the plunger for a pressure ratio of 31/11 bar and a stroke of y = 0.2 mm.

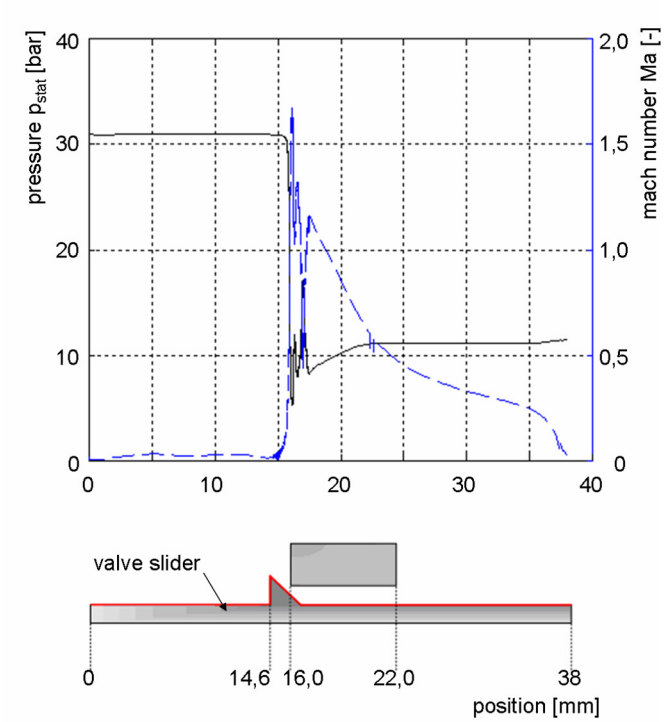

Figure 9: Static Pressure and Mach Number on valve slider

In the narrowest cross-section the fluid is accelerated to the speed of sound while the static pressure drops according to Bernoulli's energy equation. In this region the fluid will attain the critical gas flow conditions of a one-dimensional stream filament geometry. Accordingly, Mach 1 is attained at the critical pressure ratio pkrit, as is evident from Fig. 9. This diagram shows the pressure and Mach number distribution over the valve cone and the plunger surface below the valve bore for a pressure ratio of 31/11 and a stroke of 0,2 mm, identifying the position of the compression shocks on the basis of the curves of the two parameters.

Downstream of the restricting cross-section, another expansion to supersonic speed occurs until the flow is once more decelerated by a shock. As a result, the fluid is compressed to a smaller specific volume in the region of x=16mm (Fig. 10) while its velocity drops to the subsonic level and the static pressure decreases [6]. This process involves a rise in both entropy and enthalpy, since only a portion of the kinetic energy can be recovered through expansion. Following the compression, the gas accelerates to supersonic speed again before being decelerated once more by another compression shock. Once this cycle has repeated itself for the third time, the fluid expands to the counterpressure of 11 bar.

The site and frequency of the compression shocks depends on the pressure ratio and on the plunger stroke.

From the graphs we can derive a number of observations. Thus, across all pressure and stroke variations, the first compression shock occurs once the fluid has passed the narrowest cross section. The site of this shock shifts further downstream as the pressure ratio increases. Another compression shock always sets in at the point of transition from the valve cone to the adjoining plunger surface. The significant effect of a geometrical discontinuity can be assumed to be at work here. Furthermore, a comparison of the graphs shows that the qualitative evolution of the 'pressure' and 'Mach number' parameters is approximately the same for the respective pressure conditions, implying independence of the stroke.

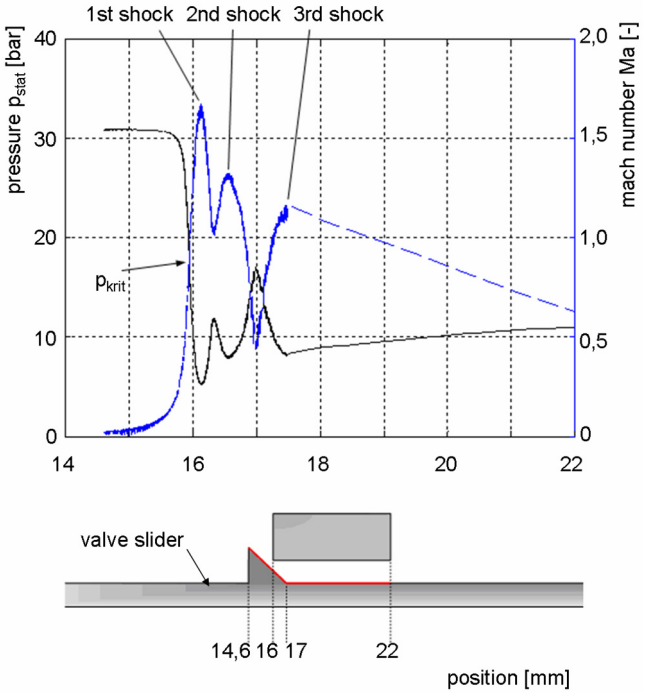

Figure 10: Static Pressure and Mach Number (Detail)

Flow Separation

The presence of decelerating boundary layers on a wall may result in flow separation and vortex formation. The pressure drop against the direction of flow decelerates the movement of the fluid. While the flow in the boundary layer stagnates or is reversed, the free flow remains unaffected by potential effects of this type due to its higher level of kinetic energy. An additional accumulation of decelerated fluid particles between the wall and the outer flow enlarges the reversed flow portion

and hence, causes a separation of the outer flow region. The separation layer thus formed can curl up into one or more vortices [7].

Moreover, the separation of flow from the wall may be the result of a compression shock in that the sudden pressure rise causes a separation of the boundary layer. In the present case the flow separation appears to be due to both effects, i.e., the pressure drop against the fluid direction and the shock/boundary layer interaction.

The flow separation and vortex formation described above lead to a constriction of the main flow known as "jet contraction". This implies that the cross-section in which fluid flow effectively occurs is narrower than the geometrical cross-section. A graphic analysis of our simulations has shown that as the pressure differential increases, the real narrowest flow cross-section changes so as to become similar to the geometrical cross section. In Fig. 11, the narrowest cross-section is determined on the basis of the critical pressure ratio.

According to [5], π_{krit} for dry air having an isentropic expansion factor $\kappa = 1.4$ can be stated as:

$$\pi_{krit,air} = \left(\frac{2}{\kappa+1}\right)^{\frac{\kappa}{\kappa-1}} = 0{,}52828 \tag{9}$$

Consequently, according to [5], the pressure pvc in the narrowest cross-section can be written thus for a primary pressure of (a) 21 bar and (b) 41 bar, respectively:

$$\text{a: } p_{vc,a} = 11{,}0939\,bar$$

$$\text{b: } p_{vc,b} = 21{,}6596\,bar$$

Assuming that the narrowest cross-section is obtained at the critical pressure ratio, the former can be expressed using the values previously determined in Fig. 11. Accordingly, as the pressure difference rises, the jet contraction zone reverts towards coinciding with the geometrically narrowest cross-section.

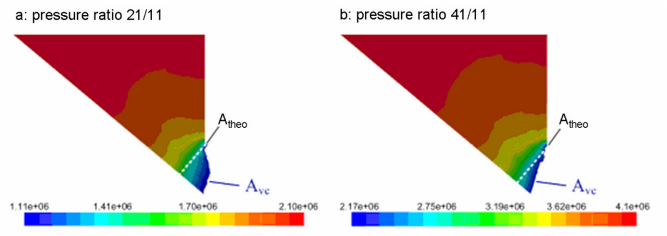

Figure 11: Geometric and Real Flow Cross-Section

Another effect of the flow reversal is the deceleration of the fluid entering over the valve seat, which involves an increase in its kinetic energy. A visualization of the velocity vectors in the plane of symmetry over the plunger illustrates this process; it is shown in Fig. 12 for a pressure ratio of (a) 21/11 and (b) 41/11 at a stroke of 0.1 mm. The symbol y_w denotes a variable characterizing the vortex pattern.

On principle it may be stated that the influence of vortex formation diminishes as the pressure differential increases. This rule is confirmed by the data from the experimental analyses described in section 6.3. According to these findings, the flow coefficient grows with increasing pressure ratio.

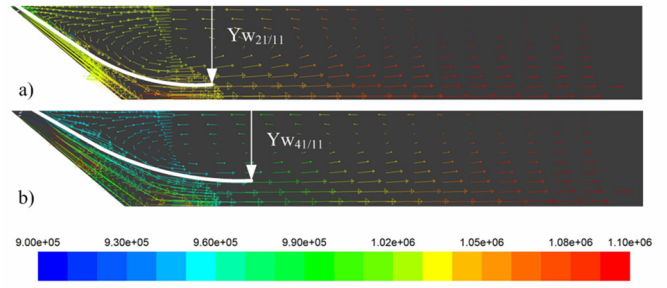

Figure 12: Eddys and Back Flow

The above-described theory regarding the origin of the reversed flow is verified in Fig. 12. The process is illustrated by the coloured velocity vectors. The presence of a pressure differential opposed to the flow direction is evident.

Vertebration in the Pressure Chambers

From the flow paths of the inflowing fluid, as shown in Fig. 13, it is possible to examine its passage through the flow domain. The colours do not reflect any physical variables; each track line has merely been coloured differently for the sake of visual contrast. While the dark-grey background areas characterize the planes of symmetry, the valve plunger is shown in light grey.

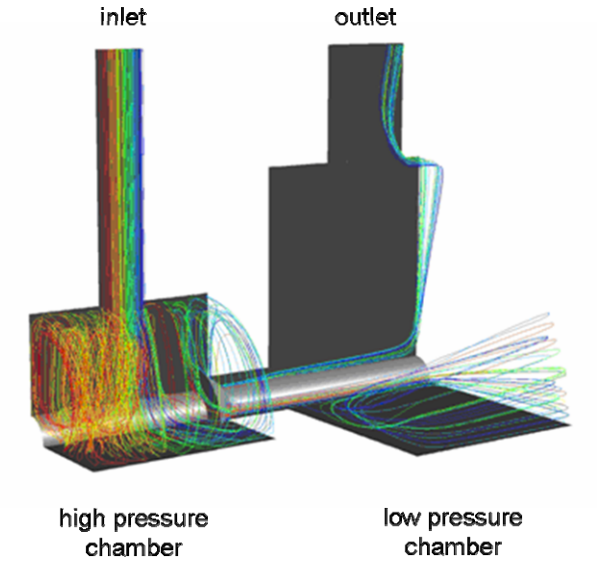

Figure 13: Visualization of Fluid Elements

Having passed the inlet, the fluid hits the plunger and is deflected towards the wall along which it then flows upwards. At the inlet / high pressure chamber interface, the flow adhering

to the wall and the incoming fluid collide; this results in the formation of a vortex zone. In the course of this process, a part of the kinetic energy carried by the inflowing fluid is transferred to the vortices. Inside the vortex zone, the processes described in the previous section take place. Due to the instable flow, smallish turbulence elements are produced continuously until the velocity gradients of these smallest movements become so steep that dissipation occurs.

A similar process takes place in the low-pressure chamber. Having passed the control edge, the fluid flows along the plunger and, upon impacting on the wall, separates into two jets. Part of the fluid flows along the wall towards the outlet while on the other hand, vortex formation occurs although to a less substantial extent than in the high-pressure chamber.

SIMULAITON BASED GEOMETRY VARIATION

In order to examine the influence of system geometry on the flow pattern, the valve design was systematically varied throughout the simulation process. This investigation was focused on factors influencing the plunger forces. The initial geometry was varied in the following manner:

- Variation of the plunger cone angle: 40°, 60° and 80°
- Introduction of a bevel to the valve bore: 0.25 and 0.50 x 45°
- Use of a radius in cone/plunger transition area: R1 and R2
- Reduction in chamber diameter by 50%
- Reduction in chamber length by 50%
- Use of a diffuser-type valve bore design

Variation of the plunger cone angle: 40°, 60° und 80°

Fig. 14 shows the computed volume flow rates, the resulting plunger forces, and the calculated flow coefficient as a function of the plunger cone angle.

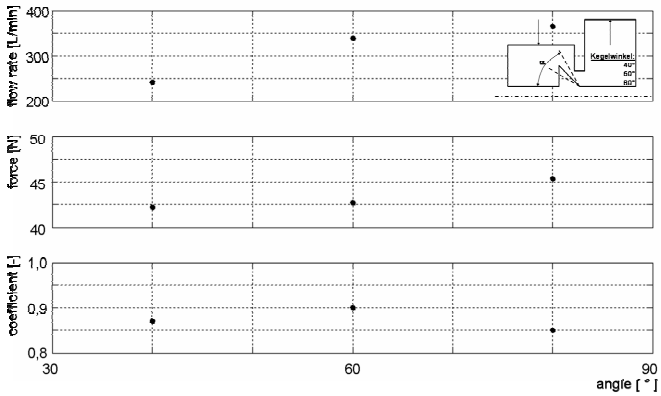

Figure 14: Variation of Valve Cone Angle

It emerges that larger cone angles will generally result in higher volume flow rates with a given unchanged plunger stroke. This rule reflects the established correlation between the cone angle and the cross-sectional area of flow as expressed in Equation (5).

As for the plunger forces, these too evidently grow as the cone angle increases.

The flow coefficients vary slightly; at a cone angle of 60° the coefficient reaches its maximum [7]. Summing up, it can be stated that the cone angle should range between 40° and 60° in the case examined here. It is thus possible to achieve low plunger forces at good flow coefficients. The resulting volume flow rates vary strongly and would have to be adapted to the specific requirements.

Introduction of a bevel to the valve bore: 0.25 und 0.50x45°

A "sharp" edge on the valve seat gives rise to linear contact and hence, higher loads on the sealing element. This load can be reduced by bevelling off the valve bore. The influence of this geometry on the valve properties examined here is demonstrated in Fig. 15.

The simulation results show an enormous increase in the plunger force, with a concurrent rise in the flow coefficient and the volume flow rate (with a 40° cone angle and a 45° bevel, the cross-sectional area of flow remains constant at the same stroke).

From the above it can be concluded that a bevel, if provided at all or imposed by production requirements, should be minimized in any event.

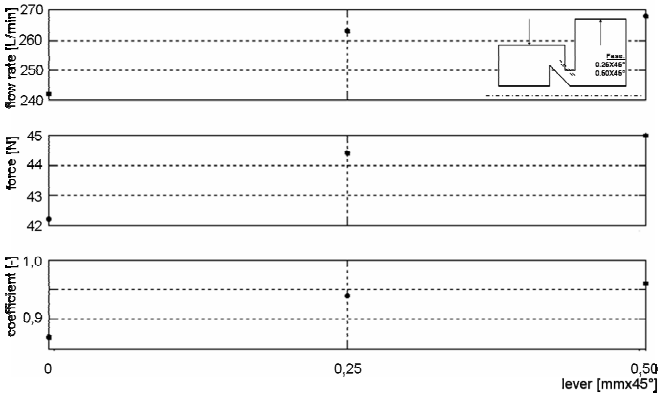

Figure 15: Variation of Valve Bung Bevel

Use of a radius in cone/plunger transition area: R1 and R2

In order to determine the influence of a radius in the cone/plunger transition area on the flow situation, the sharp edge was removed and a radius was adopted in the modelled flow geometry. The impact of this modification on the volume flow rate, plunger force and flow coefficient is illustrated in Fig. 16.

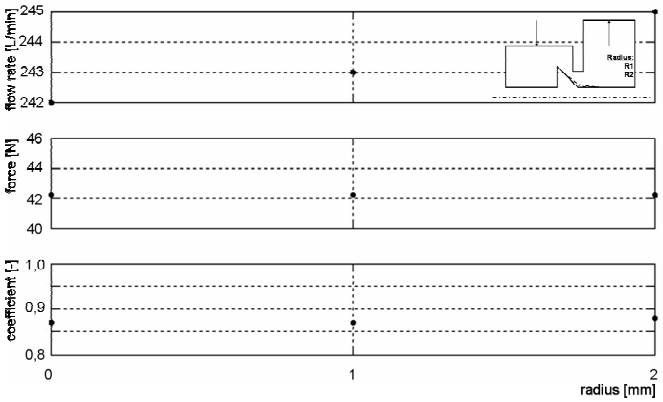

Figure 16: Variation of Cone-Slider Radius

It emerges that the plunger force is in no way influenced by this radius geometry. On the other hand, the radius increases the volume flow rate, and hence the flow coefficient, to a minor extent.

Apart from the global parameters investigated, an examination of the compression shocks above the plunger reveals a particularity which is detailed in Figs. 17 and 18.

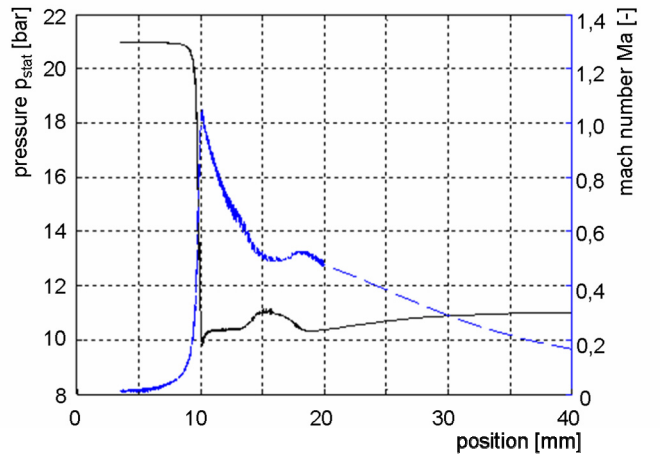

Figure 17: Static Pressure and Mach Number (R1)

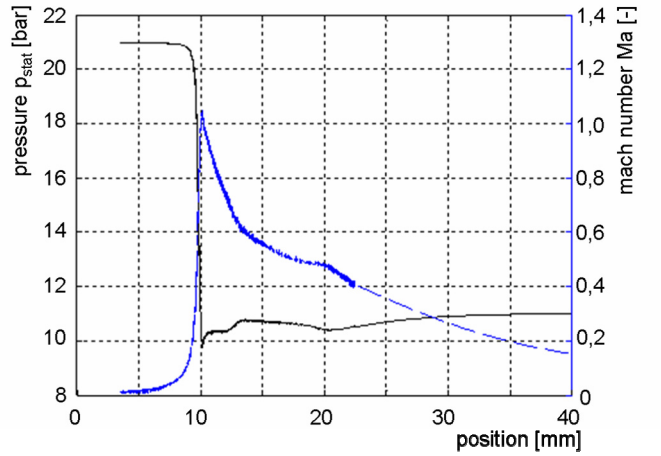

Figure 18: Static Pressure and Mach Number (R2)

It can be readily appreciated that, as a result of the radius, pronounced compression shocks no longer occur so that the flow restriction in its entirety proceeds more smoothly and more harmoniously. This has a beneficial effect on the noise formation associated with the flow restriction.

In all, it must be noted that a radius in the cone/plunger area constitutes an effective means of improving the flow characteristics while exhibiting no disadvantages in terms of the plunger forces and flow coefficients.

Reduction in chamber diameter ba 50%

Reducing the chamber diameter by half, at unchanged length, showed no tangible effect on the global parameters or flow characteristics.

Reduction in chamber lengths by 50%

This geometrical variation had no effect on the global parameters (i.e., volume flow rate, plunger force, flow coefficient). On the other hand, vortex formation in the high-pressure chamber was reduced. This phenomenon diminishes dissipation in the high-pressure chamber, which may have a beneficial effect on the flow rate at low supply pressures.

Use of a diffuser-type valve bore design

In this variation the bore was widened at a constant angle of 6°, 8° and 10°. This was expected to reduce the reverse flow effect observed.

However, the diffuser geometry failed to have the expected impact on the flow situation. On the other hand, this geometrical variation had a minor influence on the overall throughflow. A diffuser-type design of the valve bore is therefore not advisable, for the reasons outlined above.

CONCLUSION

The object of the present research was to conduct an experimental investigation and numerical simulation of the steady-state flow forces occurring on a mechatronic pressure regulator valve for natural gas powered internal combustion engines.

For the experimental determination of these forces (and of some additional flow variables), a test rig was built which, reflecting the flow geometry obtained by prior research, enabled us to carry out measurements of the global parameters for different strokes of the control element under conditions of variable supply pressure and constant counterpressure.

For the numerical simulation of our measurement series, a model was generated using the FLUENT software and was subsequently validated through comparison with the experimental results. It was found that the steady-state flow forces are highly dependent on the pressure differential across the regulator unit but correlate only to a minor extent with the mass flow conveyed. In other words, the steady-state flow forces are almost independent of the plunger stroke.

By relying on the numerical simulation, information on internal flow characteristics could be gained and first approaches towards a meaningful geometry improvement could be derived. Apart from a dissipation of flow energy due to vortex formation in the high and low pressure chambers which is imposed by the design but would be undesirable in an application case, reverse flows initiated by compression shocks were found to occur in the valve bore. This phenomenon led to diminished flow coefficients, especially at low pressure differentials, due to the contraction and deceleration of the flow entering via the plunger. With increasing pressure ratios, this jet contraction zone was found to revert to the geometrically narrowest cross-section while on the other hand, the intensity and influence of vortex formation in the valve bore was reduced.

On principle, the prevailing plunger forces are determined primarily by the pressure differential across the flow restriction zone.

The flow forces occurring are negligible under the conditions examined – i.e., a gaseous fluid and "low" mass flows – and can presumably not produce instable system behaviour provided that the favoured valve seat geometry is adopted.

A radius at the cone/plunger interface may improve the flow. A similar improvement may be achieved through the use of a bevelled valve seat, although the resulting force increase needs to be noted. A "sharp-edged" transition is favoured here from the viewpoint of sealing efficiency and industrial production requirements.

The flow spaces should be kept as small as possible to ensure maximum flow guidance and hence, to prevent the formation of major vortices resulting in dissipation.

REFERENCES

[1] Pasche, E 1990, 'Strömungskräfte in Ventilen', Technische Rundschau, vol. 82, no.47, pp. 30-34

[2] Ristic, M 2000, 'Dreidimensionale Strömungsberechnungen zur Optimierung von Hydraulikventilen bezüglich der stationären Strömungskräfte', Phd thesis, RWTH Aachen

[3] Simon, C 2007, 'Strömungslehre I', lecture notes, University of Applied Sciences, Trier

[4] Paulus, T 2007, 'Prototypenentwicklung eines mechatronischen Druckreglers für erdgasbetriebene Ottomotoren', Diploma thesis, University of Applied Sciences, Trier

[5] Murrenhoff, H 1999, Grundlagen der Fluidtechnik Teil 2: Pneumatik, Wissenschaftsverlag Aachen

[6] Prandtl, L, Oswatitsch, K & Wieghardt, K 1990, Führer durch die Strömungslehre, 9th edn, Friedrich Vieweg & Sohn Verlagsgesellschaft mbH, Braunschweig

[7] Feigel, H J 1990, 'Strömungskraftkompensation in Hydraulik-Schieberventilen', 9.Aachener Fluidtechnisches Kolloquium: conference proceedings, Verein zur Förderung der Forschung und Anwendung der Hydraulik und Pneumatik e.V., Aachen, pp. 79-98

CONTACT

Harald Ortwig holds a Dipl.-Ing. (MSc) and Dr.-Ing. (PhD) degree in Mechanical Engineering from RWTH Aachen University of Technology, Germany. Currently, he is Professor at Trier University of Applied Sciences, Germany. He is acknowledged as a Publicly Certified Expert in Fluid Power and Failure Analysis and the Valuation of Machines, apart from being a member of the SAE Fluid Power Committee and Fluid Power Net International FPNI.

Dirk Hübner holds a Dipl.-Ing. degree from Trier University of Applied Sciences, Germany. His scientific interests include modelling, simulation, and applied optimization of CNG injection systems. He was a member of the scientific staff in the Fluid Power Department of that university and is currently finishing his PhD thesis.